



# Optics Letters

## Fractal superconducting nanowire avalanche photodetector at 1550 nm with 60% system detection efficiency and 1.05 polarization sensitivity

YUN MENG,<sup>1,2</sup> KAI ZOU,<sup>1,2</sup> NAN HU,<sup>1,2</sup> XIAOJIAN LAN,<sup>1,2</sup> LIANG XU,<sup>1,2</sup> JULIEN ZICHI,<sup>3</sup>   
STEPHAN STEINHAUER,<sup>3</sup> VAL ZWILLER,<sup>3</sup> AND XIAOLONG HU<sup>1,2,\*</sup> 

<sup>1</sup>School of Precision Instrument and Optoelectronic Engineering, Tianjin University, Tianjin 300072, China

<sup>2</sup>Key Laboratory of Optoelectronic Information Science and Technology, Ministry of Education, Tianjin 300072, China

<sup>3</sup>Department of Applied Physics, Royal Institute of Technology (KTH), SE-106 91 Stockholm, Sweden

\*Corresponding author: xiaolonghu@tju.edu.cn

Received 5 September 2019; revised 5 December 2019; accepted 11 December 2019; posted 11 December 2019 (Doc. ID 377228); published 10 January 2020

**Superconducting nanowire (nanostrip) single-photon detectors (SNSPDs) have shown unprecedented detection efficiency and timing properties, but simultaneously achieving polarization-insensitive high detection efficiency, low dark-count rate (DCR), fast speed, and low timing jitter remains a challenge. Here we report on our design, fabrication, and characterization of a cascaded superconducting avalanche photodetector composed of 40 nm wide NbTiN nanowires patterned into fractal curves. At the base temperature of 2.7 K, the device exhibits  $60 \pm 3\%$  system detection efficiency at the wavelength of 1550 nm, 1.05 polarization sensitivity, 220 cps DCR, 4 ns recovery time, and 45 ps timing jitter. This Letter not only demonstrates these combined properties on a single detector that was unobtainable previously, but also shows that that current-crowding effect remarkably permits decent internal detection efficiency. These counter-intuitive results expand the understanding pertaining to the device physics of SNSPDs.** © 2020 Optical Society of America

<https://doi.org/10.1364/OL.377228>

Superconducting nanowire (nanostrip) single-photon detectors [1] (SNSPDs) have shown over 90% detection efficiency at the wavelength of 1550 nm [2–5] and superior timing performance, including fast speed [6,7] and low timing jitter [3,8]. The widely used device structure, the nanowire-meander structure, makes the detection efficiency polarization-dependent: the detector dominantly responds to the photons polarized along the nanowire. So far, several approaches have been demonstrated for reducing the polarization sensitivity [9–16]; however, achieving low polarization sensitivity while simultaneously preserving the merits of high system detection efficiency (SDE), low dark-count rate (DCR), fast speed, and low timing jitter remains a challenge. Indeed, in the family of SNSPDs with reduced polarization sensitivity that have been demonstrated,

the detectors based on molybdenum silicide (MoSi) [5] amorphous materials have achieved over 90% SDE, but they show relatively slow speed and high timing jitter; the detectors, based on niobium nitride (NbN) [11,14,15] and niobium titanium nitride (NbTiN) [9,16] polycrystalline materials, working at 2-K temperature range, preserve the superior timing properties but, so far, the highest SDE was 52.5% [13]. In particular, we recently proposed [17] and demonstrated [16] the fractal SNSPDs, and the measured device efficiency, excluding the coupling efficiency with an optical fiber, was over 60%, and the polarization sensitivity was 1.1. Although fractal SNSPDs exhibit several advantages, including that its low polarization sensitivity can be preserved for higher-order spatial modes in multi-mode fibers, the Achilles heel of the fractal SNSPD in our previous demonstration is that the U-turns and L-turns, all over the photo-sensitive region, constrict the bias current due to the current-crowding effect [18], thereby limiting the internal quantum efficiency,  $P_i$ , from saturation. Additionally, the reduced switching current would also increase timing jitter.

In this Letter, we eliminate this major constraint of the fractal SNSPDs by strategically designing the device structures. First, we shrunk the width of the nanowires down to 40 nm and decreased the fill factor to 1/3 so that resulting fractal SNSPDs based on ultra-narrow nanowires showed more saturated feature on the efficiency-bias curves, indicating increased  $P_i$ . Second, we designed the optical structure to maintain relatively high optical absorption for the low-fill factor nanowires. Third, we designed the avalanche structure [19,20] to compensate the otherwise deteriorating timing performance due to the reduced current in the ultra-narrow nanowires. Consequently, we simultaneously realized 60% SDE at the wavelength of 1550 nm, 1.05 polarization sensitivity, 220 cps DCR, 4 ns recovery time, and 45 ps timing jitter on a single detector. These combined properties were unobtainable previously, and also seemingly counter-intuitive, considering that the photon-sensitive region contains many U-turns and L-turns where the current-crowding

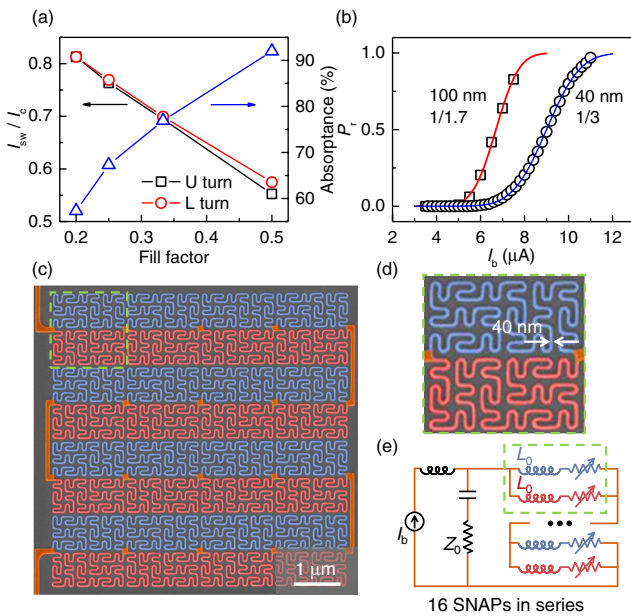


**Fig. 1.** Design and fabrication of the fractal SNAP. (a) Simulated switching current and optical absorption of the fractal-nanowire structures with different fill factors. (b) Internal quantum efficiency,  $P_r$ , of the fractal SNSPDs composed of 100 and 40 nm wide nanowires. The fill factors for the 100 and 40 nm wide nanowires are 1/1.7 and 1/3, respectively. The experimental data for the SNSPD with the 100 nm wide nanowire are from our previous work [16]. (c) False-colored SEM of the fractal SNAP, which cascades 16 2-SNAPs connected in series. (d) Zoomed-in SEM of the first 2-SNAP, and the width of the nanowire is 40 nm. (e) Equivalent circuit diagram of the SNAP. Among the 16 segments, the first one is shown inside the green dashed boxes in (c), (d), and (e).

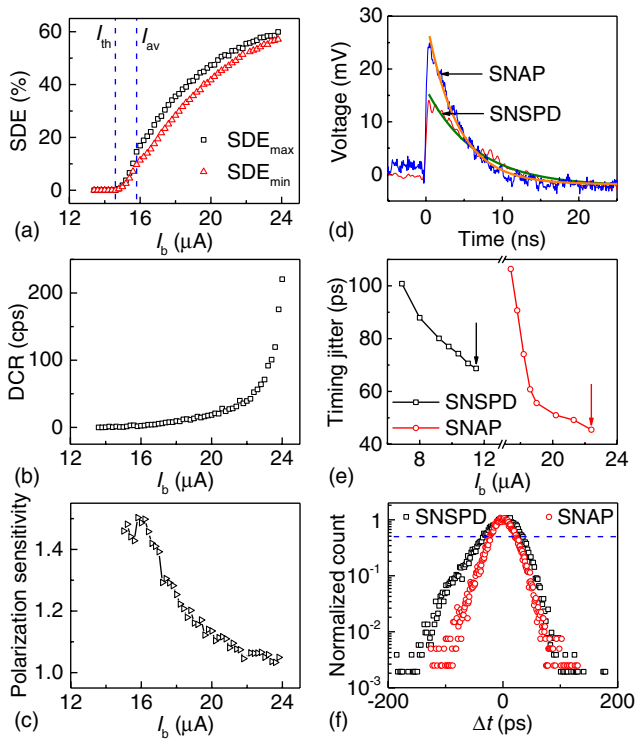
effect exists. Therefore, our results lead us to re-examine and re-evaluate the impact of the current-crowding effect in the performance of SNSPDs.

Figure 1 presents the key elements of our design and the resulting device. The tradeoffs between switching current,  $I_{sw}$ , and optical absorption,  $A$ , for fractal SNSPDs are quantified in Fig. 1(a). Increasing the fill factor increases  $A$ , but decreases  $I_{sw}$  which is limited by the U-turns, and vice versa.  $I_{sw}$  was determined by simulating the linear density of the supercurrent,  $J$ , in each structure [16,18]. The optical structure used in this Letter is similar to what we used previously [16]: the fractal nanowire is integrated in an optical microcavity with a gold mirror as one reflector and the  $\text{SiO}_2$ -Si interface as another. We used the fill factor of 1/3 so that optical absorption is 80% and  $I_{sw} = 0.69I_c$ , where  $I_c$  is the critical current of a 40 nm wide, straight nanowire. We hypothesized that decreasing the width of the nanowire can increase the  $P_r$  for fractal SNSPDs, as has been demonstrated on meander-type SNSPDs at 1550 nm [21]. Data presented in Fig. 1(b) prove this hypothesis for fractal SNSPDs. The normalized SDE of a fractal SNSPD with a nanowire width of 40 nm and a fill factor of 1/3 shows more saturated feature, and  $P_r$  was estimated to be 0.97 based on the S-shaped fitting by the error function [22],  $P_r = \frac{A_0}{2} \text{erfc}(\frac{I_{co} - I_b}{\Delta I_b})$ , where  $A_0$  and  $\Delta I_b$  are fitting parameters, and  $I_{co}$  is the inflection point of the efficiency-bias curve. In comparison, the normalized SDE of the fractal SNSPD with a nanowire width of 100 nm and a fill factor of 1/1.7 [16] shows little saturation, and an estimate of

$P_r$  is 0.83. Finally, decreasing the width of the nanowire would reduce the switching current and increase the kinetic inductance and, therefore, deteriorate the timing properties of the SNSPDs. We cascaded 16 two superconducting nanowire avalanche photodetectors (2-SNAPs) in series to double the switching current and reduce the kinetic inductance by a factor of 4, compared with those of a SNSPD with the same active area, wire width, and fill factor. Figure 1(c) presents the scanning-electron micrograph (SEM) of the cascaded SNAP we fabricated. The active area was 8.6  $\mu\text{m}$  by 8.6  $\mu\text{m}$ . Figures 1(d) and 1(e) present the zoom-in SEM of the first SNAP and the equivalent circuit of the entire device, respectively. Each SNAP as presented in Fig. 1(d) is composed of four second-order Peano curves [16]. The 9 nm thick NbTiN thin film used in this Letter [23] supported higher critical current density than the film that we used previously in Ref. [16]; the increased critical current density contributed to improving the timing performance of the resulting detectors. We used the hydrogen-silsesquioxane (HSQ) process [24,25], rather than the poly(methyl methacrylate) (PMMA) process used previously [16], to pattern the ultra-narrow nanowires.

An interesting observation, during the inspections of the HSQ structures under the scanning-electron microscope, was that with the same width of the ultra-narrow nanowires, the fractal structures were more mechanically robust than the meander structures. It is known that the adhesion of HSQ to the superconducting films is not strong [25], and fine features after exposure and development could be missing, distorted, collapsed, or drifting away, resulting in a relatively low yield of meander SNSPDs based on ultra-narrow nanowires, in particular, if the photo-sensitive area goes large. However, in contrast, the fractal structures eliminate structural orientations and, therefore, the nanomechanical forces tend to be more omnidirectional and get averaged out, which we think is the reason for the higher yield of the fractal structures based on ultra-narrow nanowires. This nanomechanical property of the fractal nanowires, in nature, is similar to the fractal metal interconnects originally used in stretchable electronics [26].

We characterized the devices in a close-cycled cryocooler at the base temperature of 2.7 K. Our setup includes a set of attocube cryogenic nano-positioners, allowing us to move a fiber focuser three-dimensionally to do *in situ* optical alignment and coupling [24]. The detector under test was illuminated from the backside through the substrate. An FC/PC vacuum feedthrough is connected with the fiber focuser inside the cryocooler and the single-mode optical fiber outside the cryocooler. The light source for measuring SDE was a pigtailed continuous-wave semiconductor laser at the wavelength of 1550 nm. A polarization controller and an in-line polarimeter module were used to control and measure the polarization state of the incident light, respectively. We defined the SDE to be the ratio of the number of output voltage pulses from the cascaded SNAP, excluding dark counts, over the number of the photons sent into this single-mode fiber, during a certain time span. We biased the detector at 23.2  $\mu\text{A}$ , scanned the polarization states of the input light over the Poincaré sphere, found the polarization states corresponding to the maximum and minimum counting rates; then, at these two polarization states, we measured the SDE as a function of the bias current. Figure 2(a) presents the measured polarization-maximum and polarization-minimum SDE, as functions of the bias current.  $I_{sw}$  of this cascaded SNAP was 23.8  $\mu\text{A}$ ; the avalanche current,  $I_{av}$ , was 15.8  $\mu\text{A}$ , comparable



**Fig. 2.** Characterization of the fractal SNAP. (a) Measured polarization-maximum and polarization-minimum SDE; (b) measured DCR; (c) residual polarization sensitivity; (d) traces of the output voltage pulses of the SNAP and the SNSPD; (e) measured timing jitter of the SNAP and the SNSPD as functions of bias current; (f) time-delay histograms of the SNAP and the SNSPD plotted in a semi-logarithms coordinate system. The full widths at half-maximum show timing jitters of 45 and 69 ps for the SNAP and the SNSPD, respectively.

with the simulated value, 15.9  $\mu\text{A}$ , from the electro-thermal simulation [27,28]; the threshold current,  $I_{\text{th}}$ , was 14.6  $\mu\text{A}$ , comparable with the simulated value, 14.9  $\mu\text{A}$ .  $I_{\text{av}}$  and  $I_{\text{th}}$  separate three bias regions: a single-photon avalanche region, where  $I_{\text{av}} < I_b < I_{\text{sw}}$ ; a two-photon avalanche region, where  $I_{\text{th}} < I_b < I_{\text{av}}$ ; and a quenched region, where  $I_b < I_{\text{th}}$ . In the single-photon avalanche region, a photon absorbed by either arm of a 2-SNAP among the 16 would trigger an avalanche and output a pulse. In the two-photon avalanche region, a single absorbed photon cannot trigger an avalanche, but can redistribute the bias current that is then latched to a steady state; if a second photon is subsequently absorbed by another arm of the same 2-SNAP, it can push forward the electro-thermal evolution and launch a complete avalanche. In the quenched region, the bias current is so low that even two photons cannot synergistically complete the avalanche process and, therefore, no output voltage pulses. In this quenched region, processes involving more photons might be able to trigger the avalanche, but the probability of multi-photon process is low. Therefore, we neglect these processes.

At the bias current of 23.2  $\mu\text{A}$ , the measured polarization-maximum SDE was  $60 \pm 3\%$ , and the polarization-minimum SDE was  $57 \pm 3\%$ . The uncertainties on the measurement of SDE are primarily from the uncertainties in output power of the laser ( $\pm 0.25\%$ ), attenuation of the variable optical attenuator

( $\pm 4.7\%$ ), and optical power measured by the optical power meter ( $\pm 1\%$ ), as well as the intrinsic shot noise, which was negligibly small. A quadratic summation of these uncertainties gives us the relative uncertainty of the SDE,  $\pm 5\%$ . Therefore, the uncertainty of the 60% and 57% SDE is  $\pm 3\%$ . Figure 2(b) presents the DCR as a function of the bias current; the maximum DCR is 220 cps, which is the lowest among polycrystalline SNSPDs with polarization-insensitive designs [11,13,15,16]. The polarization sensitivity was calculated to be 1.05. We currently have not managed to spot the specific origin of this residual polarization sensitivity, but the plot of the polarization sensitivity as a function of the bias current in Fig. 2(c) clearly shows that the residual polarization sensitivity is intrinsic to the device under test or, at least some portion is from the remaining polarization dependence of  $P_r$ . Furthermore, our measurements on fractal SNAPs and fractal SNSPDs always show the nearly monotonically increase of the residual polarization sensitivity as we decrease the bias current. This feature, of course, also appeared in meander-type SNSPDs that we made and that were made by other researchers [29], and the increase of polarization sensitivity as we decrease the bias is generally much steeper.

Figures 2(d)–2(f) present the timing properties of the fractal SNAP and the comparison with the fractal SNSPD with the same width and fill factor. The active area of the SNSPD used in comparison is 6.4  $\mu\text{m}$  by 6.4  $\mu\text{m}$ , smaller than the active area of the SNAP. The output pulses were amplified by a room-temperature RF amplifier with a bandwidth of 0.1–4 GHz and 29 dB gain, and their time-domain traces were recorded by a Le-Croy oscilloscope with a bandwidth of 4 GHz. As shown in Fig. 2(d), exponential fittings to the falling edges show  $e^{-1}$  time constants of 4.0 and 6.6 ns for the SNAP and the SNSPD, respectively. The SNAP shows faster recovery as the total kinetic inductance is less. We measured the timing jitter by employing a mode-locked, femtosecond fiber laser with the central wavelength at 1560 nm and a fast photodetector with a 3 dB bandwidth of 40 GHz. Figure 2(e) presents the results of jitter measurement on both the SNAP and the SNSPD as functions of bias current. Each data point is the full width at half-maximum of the Gaussian fitting to the time-delay histograms. The fractal SNAP shows a minimum timing jitter of 45 ps; as a comparison, the minimum timing jitter for the fractal SNSPD was 69 ps. Figure 2(f) shows in a semi-log coordinate system the time-delay histograms of the fractal SNAP and the fractal SNSPD, each biased at  $0.99I_{\text{sw}}$ . The histogram of the SNSPD shows more non-Gaussian feature.

In the family of polarization-insensitive SNSPDs [9–16], our current demonstration has shown the highest SDE among polycrystalline SNSPDs [9,11,13–15] and low residual polarization sensitivity comparable with others' work [9,11,13–15]. Although the amorphous polarization-insensitive SNSPDs exceed in SDE [5,10], their timing performance is not as good as the timing performance of polycrystalline SNSPDs. Furthermore, our concept of fractal design can also be applied to amorphous materials, including tungsten silicide (WSi) and MoSi.

Our results show that after careful design and optimization, the current-crowding effect [18] at the U-turns and L-turns all over the photo-sensitive region of the fractal SNAP remarkably yielded decent SDE on the fractal SNAPs, leading us to re-examine and re-evaluate how the current-crowding effect impacts the SDE. Traditional understanding is that the turns

with the current-crowding effect function as constrictions that would limit the SDE [18]; of course, this understanding is more specifically for meander-type SNSPDs. However, a key structural difference exists between meander- and fractal-type SNSPDs. In the meander-type SNSPDs, the U-turns that limit the switching current of the entire device are located at the edges, but the optical mode majorly overlaps with the straight part of the nanowire, where the current density is lower than the local switching current density that the straight nanowire could support. Therefore, the U-turns at the edges limit the detection efficiency of the entire device. In contrast, in the fractal SNSPDs or SNAPs, the U-turns and L-turns with the current-crowding effect distribute across the photo-sensitive area of the detector, where the local switching current is close to the switching current of the entire device, and the local DE at these turns is presumably decent. Therefore, this structural difference between fractal- and meander-type SNSPDs brings a different impact of the current-crowding effect on the overall SDE.

In summary, we have demonstrated a fractal SNAP with the following combined characteristics:  $60 \pm 3\%$  SDE at the wavelength of 1550 nm, 1.05 polarization sensitivity, 220 cps DCR, 4 ns recovery time, and 45 ps timing jitter. We believe that the fractal SNAPs will find applications where both polarization-insensitive SDE, high counting rate, and high timing resolution are crucial.

**Funding.** National Natural Science Foundation of China (11527808, 61505141); Natural Science Foundation of Tianjin City (19JCYBJC16900, 15JCYBJC52500).

**Acknowledgment.** The authors thank Dr. Weijie Sun for technical assistance in scanning-electron beam lithography and Lanqin Yan for technical assistance in e-beam evaporation.

**Disclosures.** The authors declare no conflicts of interest.

## REFERENCES

- G. Gol'tsman, O. Okunev, G. Chulkova, A. Lipatov, A. Semenov, K. Smirnov, B. Voronov, A. Dzardarov, C. Williams, and R. Sobolewski, *Appl. Phys. Lett.* **79**, 705 (2001).
- F. Marsili, V. B. Verma, J. A. Stern, S. Harrington, A. E. Lita, T. Gerrits, I. Vayshenker, B. Baek, M. D. Shaw, R. P. Mirin, and S. W. Nam, *Nat. Photonics* **7**, 210 (2013).
- I. E. Zadeh, J. W. Los, R. B. Gourgues, V. Steinmetz, G. Bulgarini, S. M. Dobrovolskiy, V. Zwiller, and S. N. Dorenbos, *APL Photonics* **2**, 111301 (2017).
- W. Zhang, L. You, H. Li, J. Huang, C. Lv, L. Zhang, X. Liu, J. Wu, Z. Wang, and X. Xie, *Sci. China Phys. Mech. Astron.* **60**, 120314 (2017).
- D. V. Reddy, R. R. Nerem, A. E. Lita, S. W. Nam, R. P. Mirin, and V. B. Verma, *Conference on Lasers and Electro-Optics (CLEO): QELS Fundamental Science* (Optical Society of America, 2019), paper FF1A-3.
- J. Münzberg, A. Vetter, F. Beutel, W. Hartmann, S. Ferrari, W. H. Pernice, and C. Rockstuhl, *Optica* **5**, 658 (2018).
- W. Zhang, J. Huang, C. Zhang, L. You, C. Lv, L. Zhang, H. Li, Z. Wang, and X. Xie, *IEEE Trans. Appl. Supercond.* **29**, 2200204 (2019).
- B. A. Korzh, Q. Y. Zhao, S. Frasca, J. P. Allmaras, T. M. Autry, E. A. Bersin, M. Colangelo, G. M. Crouch, A. E. Dane, T. Gerrits, F. Marsili, G. Moody, E. Ramirez, J. D. Rezac, M. J. Stevens, E. E. Wollman, D. Zhu, P. D. Hale, K. L. Silverman, R. P. Mirin, S. W. Nam, M. D. Shaw, and K. K. Berggren, "Demonstrating sub-3 ps temporal resolution in a superconducting nanowire single-photon detector," arXiv:1804.06839 (2018).
- S. Dorenbos, E. Reiger, N. Akopian, U. Perinetti, V. Zwiller, T. Zijlstra, and T. Klapwijk, *Appl. Phys. Lett.* **93**, 161102 (2008).
- V. B. Verma, F. Marsili, S. Harrington, A. E. Lita, R. P. Mirin, and S. W. Nam, *Appl. Phys. Lett.* **101**, 251114 (2012).
- D. Henrich, L. Rehm, S. Dörner, M. Hofherr, K. Il'in, A. Semenov, and M. Siegel, *IEEE Trans. Appl. Supercond.* **23**, 2200405 (2013).
- V. B. Verma, B. Korzh, F. Bussières, R. D. Horansky, S. D. Dyer, A. E. Lita, I. Vayshenker, F. Marsili, M. D. Shaw, H. Zbinden, R. P. Mirin, and S. W. Nam, *Opt. Express* **23**, 33792 (2015).
- J. Huang, W. J. Zhang, L. X. You, X. Y. Liu, Q. Guo, Y. Wang, L. Zhang, X. Y. Yang, H. Li, Z. Wang, and X. M. Xie, *Supercond. Sci. Technol.* **30**, 074004 (2017).
- R. Xu, F. Zheng, D. Qin, X. Yan, G. Zhu, L. Kang, L. Zhang, X. Jia, X. Tu, B. Jin, W. Xu, J. Chen, and P. Wu, *J. Lightwave Technol.* **35**, 4707 (2017).
- A. Mukhtarova, L. Redaelli, D. Hazra, H. Machhadani, S. Lequien, M. Hofheinz, J.-L. Thomassin, F. Gustavo, J. Zichi, V. Zwiller, E. Monroy, and J.-M. Gérard, *Opt. Express* **26**, 17697 (2018).
- X. Chi, K. Zou, C. Gu, J. Zichi, Y. Cheng, N. Hu, X. Lan, S. Chen, Z. Lin, V. Zwiller, and X. Hu, *Opt. Lett.* **43**, 5017 (2018).
- C. Gu, Y. Cheng, X. Zhu, and X. Hu, *Novel Optical Materials and Applications* (Optical Society of America, 2015), paper JM3A-10.
- J. R. Clem and K. K. Berggren, *Phys. Rev. B* **84**, 174510 (2011).
- R. Murphy, M. Grein, T. Gudmundsen, A. Mccaughan, F. Najafi, K. K. Berggren, F. Marsili, and E. Dauler, *Conference on Lasers and Electro-Optics (CLEO): QELS Fundamental Science* (Optical Society of America, 2015), paper FF2A.3.
- S. Miki, M. Yabuno, T. Yamashita, and H. Terai, *Opt. Express* **25**, 6796 (2017).
- F. Marsili, F. Najafi, E. Dauler, F. Bellei, X. Hu, M. Csete, R. J. Molnar, and K. K. Berggren, *Nano Lett.* **11**, 2048 (2011).
- A. Kozorezov, C. Lambert, F. Marsili, M. Stevens, V. Verma, J. Allmaras, M. Shaw, R. Mirin, and S. W. Nam, *Phys. Rev. B* **96**, 054507 (2017).
- H. Machhadani, J. Zichi, C. Bougerol, S. Lequien, J.-L. Thomassin, N. Mollard, A. Mukhtarova, V. Zwiller, J.-M. Gérard, and E. Monroy, *Supercond. Sci. Technol.* **32**, 035008 (2018).
- X. Hu, T. Zhong, J. E. White, E. A. Dauler, F. Najafi, C. H. Herder, F. N. Wong, and K. K. Berggren, *Opt. Lett.* **34**, 3607 (2009).
- X. Hu, "Efficient superconducting-nanowire single-photon detectors and their applications in quantum optics," Ph.D. thesis (Massachusetts Institute of Technology, 2011).
- J. A. Fan, W.-H. Yeo, Y. Su, Y. Hattori, W. Lee, S.-Y. Jung, Y. Zhang, Z. Liu, H. Cheng, L. Falgout, M. Bajema, T. Coleman, D. Gregoire, R. J. Larsen, Y. Huang, and J. A. Rogers, *Nat. Commun.* **5**, 3266 (2014).
- J. K. W. Yang, A. J. Kerman, E. A. Dauler, V. Anant, K. M. Rosfjord, and K. K. Berggren, *IEEE Trans. Appl. Supercond.* **17**, 581 (2007).
- F. Marsili, F. Najafi, C. Herder, and K. K. Berggren, *Appl. Phys. Lett.* **98**, 093507 (2011).
- Q. Guo, H. Li, L. You, W. Zhang, L. Zhang, Z. Wang, X. Xie, and M. Qi, *Sci. Rep.* **5**, 9616 (2015).